RESEARCH ARTICLE

New Insights into Alkali Metal Tungstates: The High Temperature Polymorphism of Na_2WO_4, the New Polymorph Li_2WO_4-V and the Redetermined Crystal Structure of $Li_2W_2O_7$

Matthias Hämmer[a] and Henning A. Höppe*[a]

Dedicated Prof. Dr. Caroline Röhr on the Occasion of her 60th birthday

Trimorphous temperature-dependent polymorphism (I: above 591°C, II: 589-591°C, III: below 589°C) was confirmed for sodium tungstate Na_2WO_4 using DSC and temperature-programmed powder XRD. Na_2WO_4-I crystallises in space group *Fddd* (no. 70, $a = 650.28(1)$, $b = 1285.12(3)$, $c = 1105.26(2)$ pm, 63 rparam., $R_{Bragg} = 0.008$), for Na_2WO_4-II a unit cell is suggested. Moreover, the crystal structure of the new triclinic polymorph Li_2WO_4-V prepared employing a LiF flux was elucidated in space group $P\bar{1}$

(no. 2, $a = 527.45(2)$, $b = 777.69(3)$, $c = 797.31(3)$ pm, $\alpha = 105.835(2)$, $\beta = 103.391(2)$, $\gamma = 90.581(2)°$, 1080 irefl., 100 param., $wR_2 = 0.063$). Finally, the crystal structure of $Li_2W_2O_7$ crystallising in space group $P\bar{1}$ (no. 2, $a = 505.57(1)$, $b = 705.00(2)$, $c = 829.03(2)$ pm, $\alpha = 69.646(1)$, $\beta = 77.868(1)$, $\gamma = 77.868(1)°$, 2386 refl., 105 param., $wR_2 = 0.025$) was redetermined revealing yet unreported lithium disorder yielding new insights into its high ionic conductivity.

Introduction

The alkali metal tungstates A_2WO_4 and ditungstates $A_2W_2O_7$ ($A = $ Li, Na, K or Rb) have already been studied extensively in the early 20th century.[1,2,3,4] During our investigations on the phosphors $Na_5M(WO_4)_4$ ($M = $ Y, La–Nd, Sm–Lu, Bi)[5] we came across the high temperature polymorphism of Na_2WO_4 which is the thermal decomposition product of $Na_5M(WO_4)_4$ alongside $NaM(WO_4)_2$. Surprisingly, the crystal structure of the high temperature polymorph was not determined as yet despite being regularly discussed in the literature.[3,6–10] In the early 20th century both Boeke, and Goranson and Kracek reported Na_2WO_4 to be trimorphous.[1,3] However, out of these three polymorphs labelled as III stable below 587.6°C, II stable to 588.8°C and I stable till the melting point of 695.5°C[3] only the crystal structure of the cubic room temperature modification (III) is known.[11,12] Further, there is ambiguity in the literature whether Na_2WO_4 is tri- or dimorphous with respect to temperature. In 1975, Bottelberghs and van Buren reported a phase diagram for the Na_2WO_4-Na_2MoO_4 system based on DTA heating data[7]

updating the diagram of Boeke determined by cooling curves.[1] For orthorhombic Na_2WO_4-I the two space groups *Pnam* and *Fddd* were suggested based on powder X-ray diffraction and Raman spectroscopy data.[7–10] Herein, we report the high temperature behaviour of Na_2WO_4 using temperature pro-grammed powder X-ray diffraction along with Rietveld refinement and differential scanning calorimetry.

Moreover, there have been reported four polymorphs of Li_2WO_4. Li_2WO_4-I adopts the Be_2SiO_4 type in space group $R\bar{3}$, Li_2WO_4-II crystallises in space group $I4_1/amd$, Li_2WO_4-III in *Pnnm* and Li_2WO_4-IV in $C2/c$. In this work, we report the crystal structure of the new polymorph Li_2WO_4-V crystallising in the triclinic space group $P\bar{1}$ isotypic with $Li_{2.09}W_{0.91}Nb_{0.09}O_4$.[13]

In the course of investigations on $AM(WO_4)_2$ ($A = $ Li, Na, K; $M = $ Y, Bi, La)[14] we also obtained single-crystals of $Li_2W_2O_7$ enabling the redetermination of its crystal structure earlier reported by Okada et al.[15] including the anisotropic refinement of the lithium and oxygen atoms elucidating disorder on one lithium site. $Li_2W_2O_7$ is a promising candidate for microwave dielectric ceramics.[16] Further, it exhibits high ionic conductivity and is the starting material for the synthesis of the reduced phase $Li_{5-x}W_2O_7$ which can (de)intercalate reversibly two lithium atoms per formula unit.[17,18] Therefore, detailed knowledge about its crystal structure is essential.

[a] M. Hämmer, Prof. Dr. H. A. Höppe
Lehrstuhl für Festkörperchemie, Institut für Physik
Universität Augsburg
Universitätsstraße 1, 86159 Augsburg, Germany
E-mail: henning@ak-hoeppe.de

Results and Discussion

High Temperature Polymorphism of Na_2WO_4

There is ambiguity in the literature[1,4,7–10] on the polymorphism of Na_2WO_4 with respect to the number of polymorphs, the transition type and the crystal structure of the high temperature

polymorph or polymorphs. The first two questions were addressed by differential scanning calorimetry (DSC) on $Na_2WO_4 \cdot 2H_2O$. In agreement with earlier results[1,7,19] the dehydration and the melting point endothermic signals in the DSC curve were observed around 100 °C and at 699 °C, respectively (Figures S1 and S2 in the supplement). For the former, the simultaneously measured thermogravimetric data yield a mass loss of 10.9 wt.% in exact agreement with the expected value (10.9 wt.%). A single endothermic signal was observed during heating, whereas two were recorded during cooling. These can be explained by the above-mentioned phase transitions. Due to the small phase width of Na_2WO_4-II – 1.2 K measured by Goranson and Kracek[3] – the two transitions overlap each other in the heating curve resulting in only one endothermic event. However, they could be separated at a heating rate of 0.1 K min⁻¹ with a phase width of 2 K for $Na2WO4$-II. The DSC data at various heating and cooling rates are displayed in Figure 1. These results show that indeed three Na_2WO_4 polymorphs can be discriminated, and the ambiguity about their number can be explained by the small extent of the phase field for Na_2WO_4-II. Accordingly, this phase can easily be overlooked. The presence of two exothermic events in the DSC cooling curve indicates that both phase transitions are reversible. Correspondingly, a phase pure sample of the cubic room temperature modification Na_2WO_4-III was obtained as confirmed by PXRD (Figure S3). Further, the DSC results agree with earlier results from temperature-dependent Raman spectroscopy indicating first order phase transitions for Na_2WO_4.

As already noted by Austin and Pierce,[4] it is not possible to obtain single-crystals of the high temperature polymorphs of Na_2WO_4 by quenching indicating that both transitions are displasive and not reconstructive. Therefore, the crystal structures of the high temperature polymorphs were investigated using temperature programmed PXRD (TPXRD) depicted in Figure 2.

In accordance with the thermal analyses, after the dehydration of $Na_2WO_4 \cdot 2H_2O$ Na_2WO_4-III is present up to 600 °C. Starting at 580 °C, an accessory phase of Na_2WO_4-I is formed. At 650 °C, only this polymorph is present. The X-ray pattern at 650 °C could be indexed successfully in the orthorhombic crystal system yielding space group *Fddd*. Consequently, the crystal structure was determined by Rietveld refinement in the Na_2SO_4-V structure type, isotypic with γ-Na_2MoO_4. Details can be found in Table S1 and Figure S4. After cooling to room temperature, Na_2WO_4-III is present exclusively again. All patterns were analysed by Rietveld refinements yielding quantitative and qualitative insights into the phase evolution. Details can be found in Tables 1 and the more detailed S2 as well as Figure S4 displaying the Rietveld refinements.

The crystal structures of both, Na_2WO_4-I and Na_2WO_4-III, are discussed based on the data obtained from the Rietveld refinements at 650 °C and 560 °C, respectively (Tables S3 and S4). The latter is the last pattern of pure Na_2WO_4-III before transformation to Na_2WO_4-I. This pattern is used instead of room temperature data for the sake of better comparability.

Cubic Na_2WO_4-III crystallises in the normal spinel type. The oxygen atoms adapt a slightly distorted cubic close packing

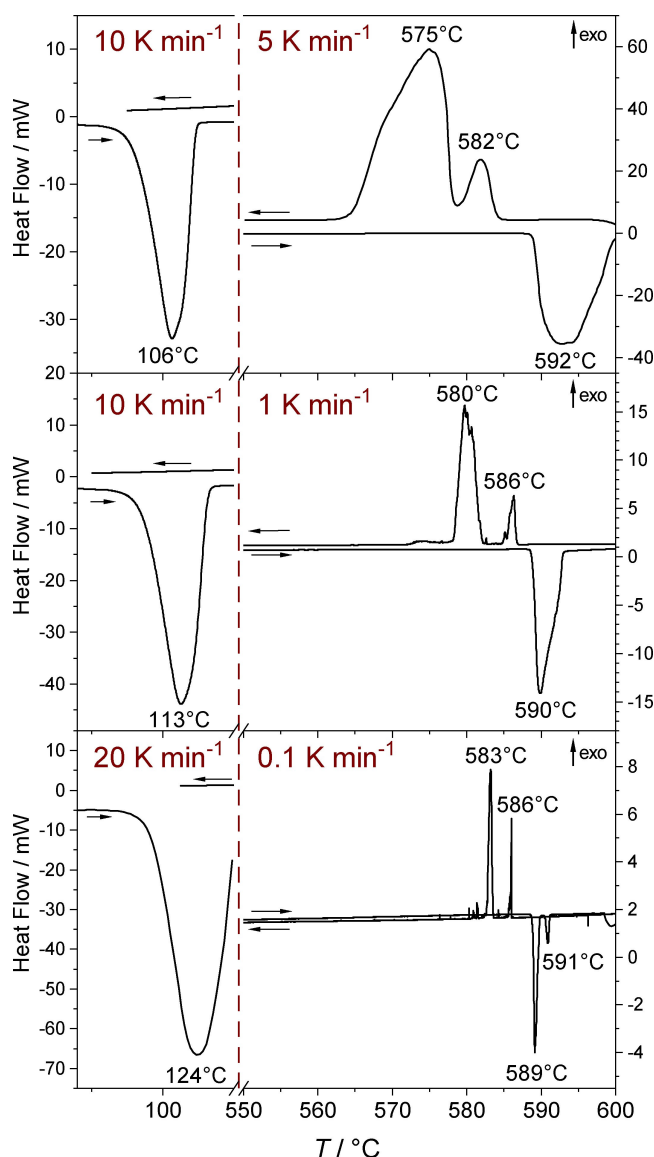**Figure 1.** DSC signals of $Na_2WO_4 \cdot 2H_2O$ for various heating and cooling rates; the endothermic event upon heating around 590 °C is split into two peaks at a slow heating rate of 0.1 K min⁻¹.

Table 1. Quantitative results of the Rietveld refinement on the TPXRD of $Na_2WO_4 \cdot 2H_2O$: The fractions are given in wt.–%; details can be found in Table S2

T / °C	30	100	560	570	580	600	650	30
$Na_2WO_4 \cdot 2H_2O$	100	0	0	0	0	0	0	0
Na_2WO_4-III	0	100	100	94	40	15	0	100
Na_2WO_4-I	0	0	0	6	60	85	100	0

with the sodium atoms in one half of the octahedral voids and the tungsten atoms in one eighth of the tetrahedral voids. This results in non-condensed WO_4 tetrahedra and NaO_6 octahedra connected via shared edges to six other NaO_6. The unit cell is shown in Figure 3a and S5. The *u* coordinate of the oxygen atoms adopts a value of approximately 0.26 instead of ¹/₄ in an
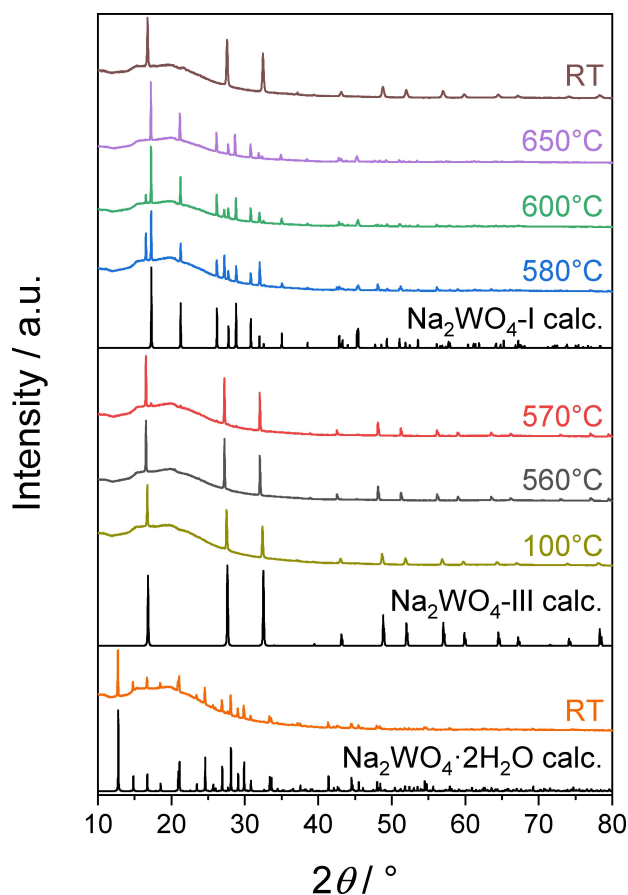
Figure 2. TPXRD of $Na_2WO_4 \cdot 2H_2O$ showing the dehydration to cubic Na_2WO_4-III, the transformation to orthorhombic Na_2WO_4-I and the recurrence of Na_2WO_4-III after cooling to room temperature.
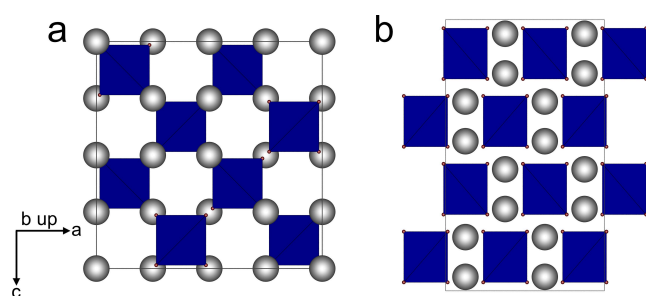

Figure 3. Unit cells of Na_2WO_4-III (a) and Na_2WO_4-I (b) viewed along [0$\bar{1}$0]; sodium atoms grey, oxygen atoms red, WO_4 tetrahedra blue.

ideal cubic closed packing resulting in slightly distorted NaO_6 octahedra with the shared edges shorter than the unshared ones. Accordingly, the deviation of these octahedra calculated by the method of Balic-Zunic and Makovicky based on all ligands enclosing spheres[20,21] from the ideal symmetry amounts to 1.9%. The WO_4 moieties show tetrahedral symmetry ($\Delta_{tetr} = 0\%$).

The crystal structure of Na_2WO_4-I comprises non-condensed WO_4 tetrahedra and highly deformed NaO_6 octahedra which are

connected to four further NaO_6 via shared edges and another four via shared corners. Each WO_4 unit coordinates two sodium atoms bidentate and eight monodentate. The unit cell is shown in Figure 3b and S6. The deviations from the ideal symmetry amount to 4.8% for the NaO_6 octahedra and 2.2% for the WO_4 tetrahedra. The sodium and tungsten atoms form chains along (001) displayed in Figure S7. For both Na_2WO_4-III and Na_2WO_4-I, the interatomic distances are in good agreement with the sum of the respective ionic radii (Tables S3 and S4).[22]

Consequently, the phase transition from Na_2WO_4-III to Na_2WO_4-I is displacive. Moreover, Na_2WO_4-I and Na_2WO_4-III are not related by a group-subgroup relation, although the space groups basically are related to each other (see remark S1 in the supplement). This indicates a discontinuous phase transition. Further, Rietveld analyses of the TPXRD yielded the volume evolution of Na_2WO_4 upon heating. Austin and Pierce reported a volume increase of 17% for the transitions III to II and a decrease of 0.12% for II to I with both transitions overlapping.[4] Our results (Table S2) show a linear increase of the unit cell volume of Na_2WO_4-III with temperature (4% at 580°C) accompanied by an increase of the average W–O bond length in accordance with results of in-situ high-temperature Raman spectroscopy.[10] Na_2WO_4-I has an increased unit cell volume of 20% compared to room temperature Na_2WO_4-III. Consequently, the results from Rietveld analysis are in good agreement with the measurement of the linear thermal expansion.[4] The unit cell parameter c is the most sensitive in Na_2WO_4-I towards temperature since sodium and tungsten atoms form chains along this direction. Further, Na_2WO_4-I shows decreased W-O distances and slightly distorted tungstate tetrahedra in accordance with Raman spectroscopy.[10]

TPXRD was also employed upon cooling (Figure S8). Here, a new phase appears to form at 560°C while Na_2WO_4-I is present at 570°C. After cooling to room temperature Na_2WO_4-III is present. The new phase might represent Na_2WO_4-II since the DSC data showed a larger phase width upon cooling in accordance with the existence of Na_2WO_4-I at 570°C. However, the structure could not be determined reliably although indexing and a Pawley fit in space group $I4_1/amd$ are possible with lattice parameters $a = 1707.2$ pm, $c = 1293.6$ pm ($R_{Bragg} = 0.013$, $R_{wp} = 0.058$, Figure S9) – $I4_1/amd$ is a maximal subgroup of $Fd\bar{3}m$ and a direct supergroup of $Fddd$. Therefore, it might be plausible that Na_2WO_4-II would crystallise in this space group, but neither between Na_2WO_4-I and Na_2WO_4-III a symmetry relationship can be derived nor fits the aforementioned unit cell into such a scheme. Noteworthy, this is also in contrast to Na_2MoO_4 with the respective phase β-Na_2MoO_4 reportedly crystallising in space group $Pbn2_1$.[7] However, no crystal structure was determined for this compound so far. Moreover, Bramnik and Ehrenberg observed similar differences in solving the structure of β-Na_2WO_4 based on TPXRD data reporting similarity of the β-Na_2MoO_4 and the γ-Na_2MoO_4 diffractograms.[23] The latter crystallises in space group $Fddd$, i.e. it is the counterpart of Na_2WO_4-I. The same holds for Na_2WO_4 and the TPXRD measurement in our contribution. The problem of obtaining Na_2WO_4-II was already observed in earlier studies both using XRD or Raman spectroscopy.[7,8,10] The major

obstacles are the very narrow phase width of only 1 to 2 K and the reversible nature of the phase transitions.

Crystal Structure of Li$_2$WO$_4$-V

Li$_2$WO$_4$-V was prepared via flux synthesis. Besides colourless single-crystals of Li$_2$WO$_4$-V, single-crystals of LiLa(WO$_4$)$_2$ were formed and an accessory phase of LaBWO$_6$ was observed (Figure S10). For the latter, unfortunately, no single-crystals
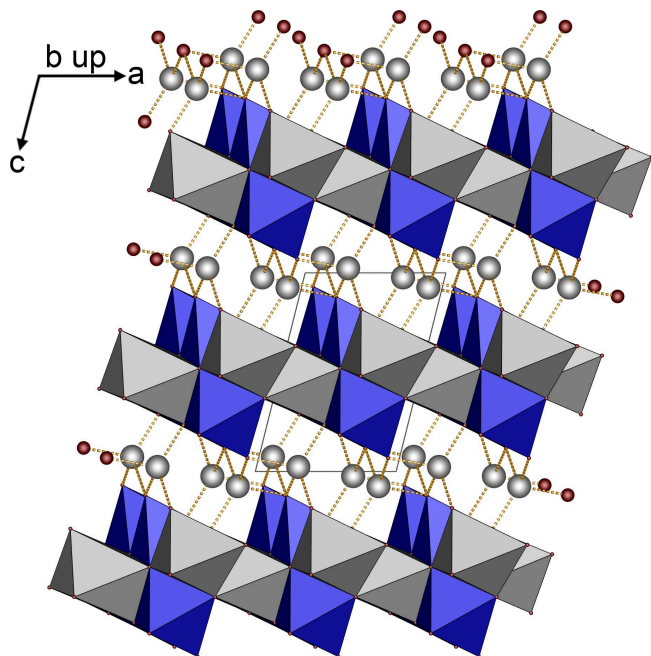

Figure 4. Layered structure of Li$_2$WO$_4$-V: Layers formed by edge sharing LiO$_6$ (grey) and WO$_6$ (blue) octahedra in the ab plane are connected via Li$_4$O$_{10}$ building units along (001); oxygen atoms red, lithium atoms grey.

were formed since this phase is awaiting the unambiguous determination of its crystal structure.[24]

Li$_2$WO$_4$-V crystallises in space group $P\bar{1}$ (no. 2) with four formula units per unit cell (Figures 4 and S11 and Tables S5 and S6) isotypically to Li$_{2.09}$W$_{0.91}$Nb$_{0.09}$O$_4$[13] and is reminiscent of a distorted inverse spinel structure. Accordingly, a distorted cubic closest packing of oxygen atoms hosts tungsten atoms in one fourth of the octahedral voids and lithium atoms in another fourth of them as well as in one eighth of the tetrahedral voids. The substructure features distinct W$_4$O$_{16}$ moieties formed by four WO$_6$ octahedra sharing two and three edges with each other, respectively (Figure 5a), distinct Li$_4$O$_{10}$ building units formed by four edge-sharing LiO$_4$ tetrahedra (Figure 4b) and layers of LiO$_6$ octahedra sharing edges (Figure S12). The latter are formed by chains of edge sharing LiO$_6$ octahedra in the [010] direction which are further connected by shared edges resulting in layers in the ab plane. Each LiO$_6$ octahedron is connected to three others. Thus, the LiO$_6$ layers contain voids in which W$_4$O$_{16}$ units are located. The LiO$_6$ and WO$_6$ octahedra are connected via shared edges. Thus, the octahedra share six or seven edges with other octahedra (W1: 3 WO$_6$, 4 LiO$_6$, W2: 2 WO$_6$, 4 LiO$_6$, Li3: 3 WO$_6$, 4 LiO$_6$, Li4: 5 WO$_6$, 2 LiO$_6$). The layers exhibiting a highly distorted variant of the layers in the CdCl$_2$ structure are connected via the Li$_4$O$_{10}$ building units along [001] resulting in a network (Figure 4). The interatomic distances are all in good agreement with the sum of the ionic radii (Table S8, Figures 5 and S12).[22] Due to the large difference in nominal charge between lithium ($+1$) and tungsten ($+6$), the respective octahedra are severely distorted. This was quantified using deviations the method of Balic-Zunic and Makovicky to calculate the deviation from the octahedral symmetry Δ_{oct}.[20,21] The LiO$_6$ octahedra show even larger deviations of 17.4 % (Li3) and 12.8 % (Li4) than the tungstate octahedra with $\Delta_{oct} = 8.7$ % (W1) and 4.2 % (W2). Also the LiO$_4$ tetrahedra deviate significantly from tetrahedral symmetry – 3.9 % for Li1 and 4.0 % for Li2 – and can therefore be considered as non-regular ones.[25] The electrostatic reasonability of the crystal structure was
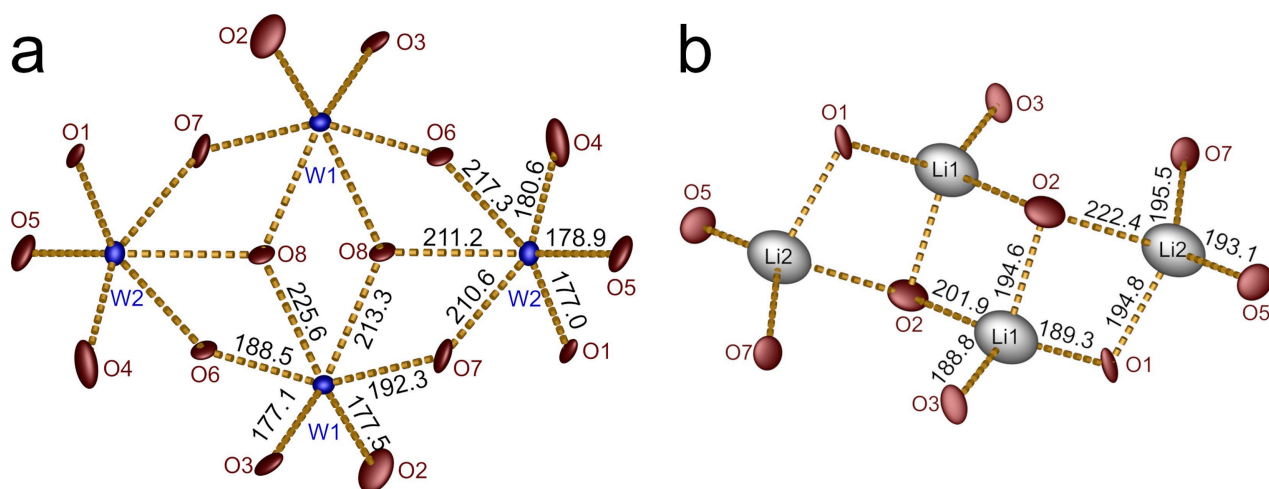

Figure 5. Distinct W$_4$O$_{16}$ (a) and Li$_4$O$_{10}$ (b) building units in Li$_2$WO$_4$-V: The ellipsoids are shown at 80 % probability; oxygen atoms red, tungsten atoms blue, lithium atoms grey; the respective distances are given in pm.

confirmed by calculations based on the MAPLE concept (MAdelung Part of Lattice Energy).[26] The MAPLE values of Li_2WO_4-V and Li_2WO_4-IV[27] were calculated and compared (Table S9). The deviation is well below 1% which is our empirical benchmark for electrostatic consistency. Moreover, all coordination numbers were confirmed by these calculations.

Compared to the four polymorphs reported in the literature for Li_2WO_4, our new Li_2WO_4-V comprises structural motifs closely related to Li_2WO_4-II and Li_2WO_4-III. The W_4O_{16} building unit can be found analogously in Li_2WO_4-III. Moreover, LiO_6 octahedra and LiO_4 tetrahedra coexist in Li_2WO_4-II. Therein, the W_4O_{16} building unit comprises four WO_6 tetrahedra all sharing three edges with the other. The tetrahedrally coordinated lithium atoms form Li_4O_{12} building units formed by four corner-sharing tetrahedra.

Crystal Structure of $Li_2W_2O_7$

Single-crystals of $Li_2W_2O_7$ were obtained as byproduct during attempts to prepare single-crystals of $LiBi(WO_4)_2$ from the melt.[14] However, phase pure $Li_2W_2O_7$ is accessible by simple solid state reaction of the educts Li_2CO_3 and WO_3 at 800 °C. The respective PXRD pattern is shown in Figure S13. The crystal structure of $Li_2W_2O_7$ was determined by Okada et al. in 1975.[15] In addition to the confirmation of the crystal structure, we could provide the anisotropic refinement of all present atoms and elucidate the disorder of the Li(2) site.

$Li_2W_2O_7$ crystallises in the triclinic space group $P\bar{1}$ (no. 2) and two formula units per unit cell as depicted in Figure 6a. The anion features two crystallographically distinct sets of WO_6 octahedra sharing three and two edges with adjacent ones according to the Niggli formalism $(W1O_{1/1}O_{3/2}O_{2/3})(W2O_{2/1}O_{3/2}O_{1/3})^{2-}$ resulting in $[W_2O_7]^{2-}$ double chains along [100]. These $[W_2O_7]_\infty$ ribbons exhibit rock salt type configuration.[17] Further, there are two crystallographically distinct tetrahedrally coordinated lithium sites, Li1 (Figure 6b) and Li2 (Figure 6c). Li2 is distributed over two sites in a ratio of 73:27. In the majority variant, both sets of LiO_4 tetrahedra share

two corners with other tetrahedra resulting in zig-zag chains along [100] (Figure S14). These chains share corners with the $[W_2O_7]^{2-}$ double chains surrounding them. Consequently, a network is formed. In the minority variant however, distinct Li_4O_{12} building units displayed in Figure S15 are stacked along [100]. In contrast to the majority variant, where each $[W_2O_7]^{2-}$ double chain is surrounded by six LiO_4 zig-zag chains, four Li_4O_{12} stacks surround each $[W_2O_7]^{2-}$ double chain in the minority variant.

Using the method of Balic-Zunic and Makovicky,[20,21] the $W1O_6$ octahedra can be considered regular ($\Delta_{oct} = 0.2\%$), whereas all other polyhedra are non-regular with deviations of Δ_{oct} (W2) = 9.7% and Δ_{tetra} ranging from 5.3 to 7.5% for the LiO_4 tetrahedra. All interatomic distances are in good agreement with the sum of the ionic radii (Table S10, Figure 6b and 6c).[22]

The electrostatic reasonability of the crystal structure was confirmed by calculations and comparison of the MAPLE values of $Li_2W_2O_7$ and the sum of those of Li_2WO_4-V and WO_3[28] (Table S9). Moreover, all coordination numbers were confirmed by our calculations.

High ionic conductivity is reported for $Li_2W_2O_7$.[17] This was attributed to the ribbon-type structure. Recently, Xu et al. investigated the ionic conductivity of $Li_2W_2O_7$ extensively.[18] Their results indicate that the ionic conductivity is dominated by the O^{2-} transport. Based on the calculation of the bond-valence-based energy landscape[29] and their structural model obtained by Rietveld refinement from powder neutron diffraction data containing intrinsic lithium and oxygen vacancies, possible Li^+ and O^{2-} migration pathways could be identified. For Li^+, interstitial sites the ions pass through to get from one lithium site to the other are reported. One of these – namely i6 – coincides well with the minority Li2 site from our structure determination. The O^{2-} migration might take place along the $[W_2O_7]_\infty$ ribbons. By hopping along the edges of the LiO_4 tetrahedra from one ribbon to another 3D migration is possible. This might be facilitated by the lithium disorder enhancing the number of possible O^{2-} pathways. Thus, the lithium disorder elucidated above can be expected to play a certain role in the
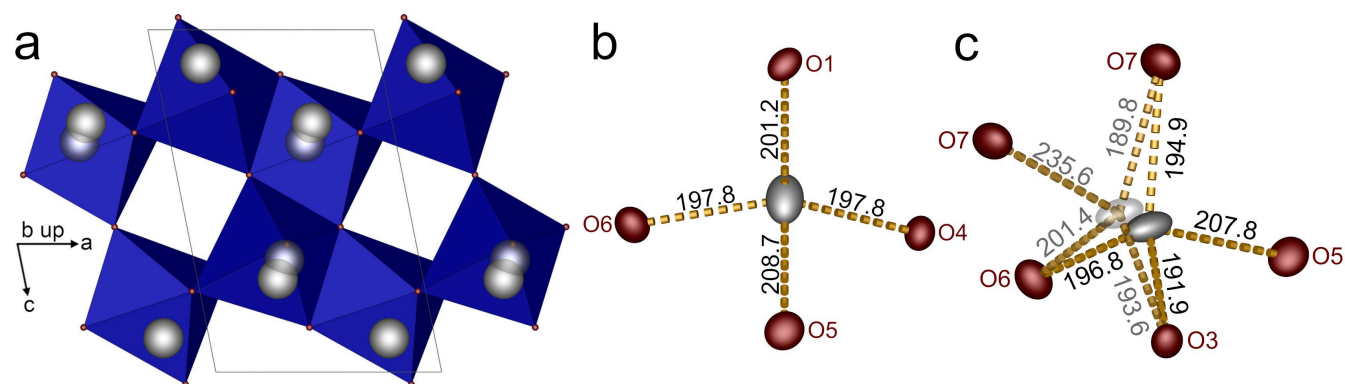

Figure 6. (a) Unit cell of $Li_2W_2O_7$ along (010): tungstate octahedra are shown in blue, oxygen atoms in red and lithium atoms in grey; for the latter, the minority variant is shown semitransparent; (b) $Li1O_4$ tetrahedron; (c) disorder of the Li2 site: the minority variant (Li2B) is shown semitransparent, the majority variant (Li2 A) opaque; the Li–O distances are given in pm; ellipsoids are shown at 80% probability.

ion transport in $Li_2W_2O_7$ yielding new insights in the migration pathways of both Li^+ and O^{2-} ions.

Conclusions

Despite over a century of research on alkali tungstates, remaining questions were identified and addressed. Trimorphous temperature-dependent polymorphism (I: 591 °C to melting point, II: 589–591 °C, III: up to 589 °C) was confirmed for sodium tungstate Na_2WO_4 using DSC and temperature-programmed powder XRD. Na_2WO_4-I crystallises in the Na_2SO_4-V structure type determined by Rietveld refinement, and for Na_2WO_4-II we suggest a tetragonal unit cell based on the TPXRD data and a space group in accordance with a symmetry relationship to Na_2WO_4-I. For Li_2WO_4, a new fifth polymorph was prepared via LiF flux and the crystal structure was determined. Li_2WO_4-V crystallises isotypically with $Li_{2.09}W_{0.91}Nb_{0.09}O_4$. Finally, the crystal structure of $Li_2W_2O_7$ was redetermined enabling the anisotropic refinement of all atoms. Moreover, lithium disorder was elucidated explaining the high ionic conductivity previously reported for this compound.

Experimental Section

Materials

$Na_2WO_4 \cdot 2H_2O$ (99 %, Fluka), La_2O_3 (99.99 %, Auer-Remy), $B(OH)_3$ (99.5 %, Merck), WO_3 (99.8 %, Alfa Aesar), LiF (97 %, Aldrich), Li_2CO_3 (99.9 %, Acros) and Bi_2O_3 (99.5 %, Riedel-de Haen) were used as starting materials without further purification and were handled in air. The respective purities are given in parentheses.

Syntheses

Li_2WO_4-V was prepared via flux synthesis. 1.16 mmol La_2O_3, 2.56 mmol $B(OH)_3$, 2.33 mmol WO_3 and 2.33 mmol LiF were ground, transferred into a platinum crucible and heated in a muffle furnace with the following program: heating to 1000 °C with 100 K h^{-1}, holding the temperature for 24 h, cooling to 750 °C with 5 K h^{-1} and further cooling to room temperature with 100 K h^{-1}. A colourless powder containing single-crystals was obtained.

$Li_2W_2O_7$ was prepared via solid state synthesis starting from 2 mmol Li_2CO_3 and 4 mmol WO_3. The starting materials were ground and transferred into a corundum crucible which was heated in a muffle furnace at 800 °C for 10 h (heating and cooling ramps 200 K h^{-1}). Single-crystals of $Li_2W_2O_7$ were obtained from the melt. Firstly, 0.28 mmol Li_2CO_3, 0.28 mmol Bi_2O_3 and 1.1 mmol WO_3 were reacted by solid state reaction by the following furnace program: 20 h at 550 °C, intermediate grinding and 25 h at 500 °C (heating and cooling ramps 200 K h^{-1}). The resulting mixture containing $Li_2W_2O_7$, $Bi_2W_2O_9$, WO_3 and $LiBi(WO_4)_2$ was heated inside a platinum crucible at 800 °C for 10 h after heating with 200 K h^{-1}. Subsequently it was cooled to 400 °C with 5 K h^{-1} and then with 200 K h^{-1} to room temperature. The product contained large single-crystals of both $Li_2W_2O_7$ and $LiBi(WO_4)_2$.

Single-Crystal X-Ray Structure Determination

Suitable single-crystals were selected for single-crystal XRD under a polarising microscope. Diffraction data were collected with a Bruker D8 Venture diffractometer using Mo−Kα radiation ($\lambda = 0.71073$ Å). Absorption correction was performed by the multiscan method. The structures were solved by Direct Methods and refined by full-matrix least-squares technique with the SHELXTL crystallographic software package.[30] Relevant crystallographic data and further details of the structure determinations are summarised in Table S5–7. For Li_2WO_4-V, the relatively large residual electron density as well as the somewhat flattened anisotropic displacement parameters of some lithium atoms are presumably due to the combination of heavy tungsten and light lithium atoms in the structure causing structure determining heavy atom centered moieties as well as respective cut-off effects. However, the precession images for this measurement show no peculiarities (Figure S16). For the same reason, only two out of the four lithium atoms could be refined anisotropically.

Further details of the crystal structure investigations may be obtained at https://www.ccdc.cam.ac.uk/ on quoting the depository numbers CSD-2126944 (Li_2WO_4-V), CSD-2126945 ($Li_2W_2O_7$), the names of the authors, and citation of this publication.

Powder X-Ray Diffraction (PXRD)

Ground samples were prepared on a stainless-steel sample holder and flattened using a glass plate. The powder X-ray diffraction patterns were measured with a Seifert 3003 TT diffractometer at room temperature in Bragg-Brentano geometry using Cu-K$_\alpha$ radiation ($\lambda = 1.54184$ Å), a GE METEOR 1D line detector and a Ni-Filter to suppress K_β radiation (X-ray tube operated at 40 kV and 40 mA, scan range: 5–80°, increment: 0.02°, 40 scans per data point, integration time: 200 s per degree, variable divergence slit).

Temperature-programmed Powder X-Ray Diffraction (TPXRD)

The samples were ground and filled into a silica-glass Hilgenberg capillary (outer diameter 0.3 mm, wall thickness 0.01 mm). The data were collected between $T = 30$ and 650 °C (2 h annealing at the respective temperature before the measurement) with a Bruker D8 Advance diffractometer with Cu-K$_\alpha$ radiation ($\lambda = 1.54184$ Å) with a 1D LynxEye detector, steps of 0.02° and transmission geometry. The generator was driven at 40 kV and 40 mA. The strong background between $12.5° < 2\theta < 30°$ is due to the used furnace attachment. The maximum temperature was set below the melting point of Na_2WO_4 due to reactions of the melt with the silica-glass capillary observed during preliminary experiments forming a significant SiO_2 side phase.

Rietveld Refinement

Analysis of diffraction data was performed using the Rietveld method with the program TOPAS V. 5.0.[31] The instrumental resolution function was determined empirically from a set of fundamental parameters using a reference scan of Si (NIST 640d).[32] The structural models of Na_2WO_4-III[11] and Na_2SO_4-V[33] were used as starting models for Rietveld analysis. The isotropic thermal displacement parameters were constrained to two common values for the heavy tungsten atoms, and the lighter sodium and oxygen atoms to minimise quantification errors. The background was modeled with a Chebychev polynomial. Details are displayed in Tables S1 and S5.

RESEARCH ARTICLE

Further details of the crystal structure structure investigations of Na_2WO_4-I and Na_2WO_4-III may be obtained at https://www.ccdc.cam.ac.uk/ on quoting the depository numbers CSD-2126943 (Na_2WO_4-I) and CSD-2126943 (Na_2WO_4-III), the names of the authors, and citation of this publication.

Thermogravimetry (TG) and simultaneous Differential-Scanning Calorimetry (DSC)

The TG and DSC analyses were performed simultaneously with a NETZSCH STA 409 PC Luxx thermobalance under N_2 atmosphere with 50 mL min^{-1} flow in platinum crucibles (heating rate: 5 K min^{-1}).

Single Differential Scanning Calorimetry (DSC)

The DSC measurements were performed on a TA Instruments DSC 2920 in a 50 mL min^{-1} N_2 flow using Netzsch standard Al pans with pierced lids with various heating and cooling rates discussed in the manuscript up to 600 °C.

Acknowledgements

Conflict of Interest

The authors declare no conflict of interest.

Data Availability Statement

The data that support the findings of this study are available from the corresponding author upon reasonable request.

[1] H. E. Boeke, *Z. Anorg. Chem.* **1906**, *50*, 355–381.
[2] a) H. S. Klooster, *Z. Anorg. Chem.* **1914**, *85*, 49–64; b) V. M. Goldschmidt, *Skr. Akad. Oslo* **1926**, *2*, 107; c) F. Hoermann, *Z. Anorg. Allg. Chem.* **1929**, *177*, 145–186.
[3] R. W. Goranson, F. C. Kracek, *J. Chem. Phys.* **1935**, *3*, 87–92.
[4] J. B. Austin, R. H. H. Pierce, *J. Chem. Phys.* **1935**, *3*, 683–686.
[5] M. Hämmer, O. Janka, J. Bönnighausen, S. Klenner, R. Pöttgen, H. A. Höppe, *Dalton Trans.* **2020**, *49*, 8209–8225.
[6] A. Vamvakeros, S. D. M. Jacques, M. Di Michiel, P. Senecal, V. Middelkoop, R. J. Cernik, A. M. Beale, *J. Appl. Crystallogr.* **2016**, *49*, 485–496.
[7] P. H. Bottelberghs, F. R. van Buren, *J. Solid State Chem.* **1975**, *13*, 182–191.
[8] C. L. Lima, G. D. Saraiva, P. T. C. Freire, M. Maczka, W. Paraguassu, F. F. de Sousa, J. Mendes Filho, *J. Raman Spectrosc.* **2011**, *42*, 799–802.
[9] C. W. F. T. Pistorius, *J. Chem. Phys.* **1966**, *44*, 4532–4537.
[10] J. Wang, J. You, M. Wang, L. Lu, A. A. Sobol, S. Wan, *J. Raman Spectrosc.* **2018**, *49*, 1693–1705.
[11] A. D. Fortes, *Acta Crystallogr. Sect. E* **2015**, *71*, 592–596.
[12] K. Okada, H. Morikawa, F. Marumo, S. Iwai, *Acta Crystallogr. Sect. B* **1974**, *30*, 1872–1873.
[13] R. Sharma, M. Lundberg, *Acta Crystallogr. Sect. C* **1985**, *41*, 173–177.
[14] V. Wessels, M. Hämmer, K. Kreß, F. Becker, H. A. Höppe, *in preparation*.
[15] K. Okada, H. Morikawa, F. Marumo, S. Iwai, *Acta Crystallogr. Sect. B* **1975**, *31*, 1451–1454.
[16] a) C.-F. Tseng, H.-C. Hsu, P.-H. Chen, *J. Alloys Compd.* **2018**, *764*, 840–844; b) J. Chen, C. Li, D. Wang, H. Xiang, L. Fang, *J. Adv. Dielect.* **2017**, *07*, 1720001.
[17] V. Pralong, G. Venkatesh, S. Malo, V. Caignaert, R. Baies, B. Raveau, *Inorg. Chem.* **2014**, *53*, 522–527.
[18] J. Xu, X. Xu, H. Yi, Y. Lv, N. Xu, L. He, J. Chen, X. Kuang, K. Huang, *Inorg. Chem.* **2021**, *81*, 2565.
[19] G. G. Guarini, L. Dei, *Thermochim. Acta* **1995**, *250*, 85–96.
[20] T. Balić Žunić, E. Makovicky, *Acta Crystallogr.* **1996**, *B52*, 78–81.
[21] E. Makovicky, T. Balić-Žunić, *Acta Crystallogr.* **1998**, *B54*, 766–773.
[22] R. D. Shannon, *Acta Crystallogr. Sect. A* **1976**, *32*, 751–767.
[23] K. G. Bramnik, H. Ehrenberg, *Z. Anorg. Allg. Chem.* **2004**, *630*, 1336–1341.
[24] a) K. K. Palkina, V. Z. Saifuddinov, V. G. Kuznetsov, B. F. Dzhurinskii, G. V. Lysanova, E. M. Reznik, *Zh. Neorg. Khim.* **1979**, *24*, 1193–1198; b) C.-X. Sun, Z.-B. Lin, L.-Z. Zhang, Y.-S. Huang, G.-F. Wang, *Chinese J. Struct. Chem.* **2013**, *32*, 1088–11092.
[25] H. A. Höppe, *J. Solid State Chem.* **2009**, *182*, 1786–1791.
[26] a) R. Hübenthal, *MAPLE. Program for the Calculation of the Madelung Part of Lattice Energy*, Universität Gießen, Gießen **1993**; b) R. Hoppe, *Angew. Chem.* **1966**, *78*, 52–63; *Angew. Chem. Int. Ed.* **1966**, *5*, 95–106; c) R. Hoppe, *Angew. Chem. Int. Ed.* **1970**, *9*, 25–34; *Angew. Chem.* **1970**, *82*, 7–16.
[27] H. Horiuchi, N. Morimoto, S. Yamaoka, *J. Solid State Chem.* **1980**, *33*, 115–119.
[28] A. Aird, M. C. Domeneghetti, F. Mazzi, V. Tazzoli, E. K. H. Salje, *J. Phys. Condens. Matter* **1998**, *10*, L569-L574.
[29] a) M. Avdeev, M. Sale, S. Adams, R. P. Rao, *Solid State Ionics* **2012**, *225*, 43–46; b) H. Chen, L. L. Wong, S. Adams, *Acta Crystallogr. Sect. B* **2019**, *75*, 18–33; c) K.-H. Park, K. Kaup, A. Assoud, Q. Zhang, X. Wu, L. F. Nazar, *ACS Energy Lett.* **2020**, *5*, 533–539.
[30] G. M. Sheldrick, *Acta Crystallogr. Sect. C* **2015**, *71*, 3–8.
[31] Bruker AXS, *Topas V5, General profile and structure analysis software for powder diffraction data. User's Manual*, Karlsruhe, Germany **2014**.
[32] R. W. Cheary, A. A. Coelho, J. P. Cline, *J. Res. Natl. Inst. Stand. Technol.* **2004**, *109*, 1–25.
[33] A. G. Nord, S. E. Sværen, J. Møller, G. Schroll, K. Leander, C.-G. Swahn, *Acta Chem. Scand.* **1973**, *27*, 814–822.